JAERI-Research
97-087

ENERGY TRANSFER AND THERMAL CONDUCTIVITY THROUGH INERT MATRIX AND NUCLEAR FUEL ANALOGOUS MATERIALS

November 1997

Claude DEGUELDRE*, Masahide TAKANO, Toshihiko OHMICHI, Kousaku FUKUDA, Peter HEIMGARTNER* and Thomas GRABER*

日本原子力研究所
Japan Atomic Energy Research Institute

本レポートは，日本原子力研究所が不定期に公刊している研究報告書です。
入手の問合わせは，日本原子力研究所研究情報部研究情報課（〒319-11 茨城県那珂郡東海村）あて，お申し越しください。なお，このほかに財団法人原子力弘済会資料センター（〒319-11 茨城県那珂郡東海村日本原子力研究所内）で複写による実費頒布をおこなっております。

This report is issued irregularly.
Inquiries about availability of the reports should be addressed to Research Information Division, Department of Intellectual Resources, Japan Atomic Energy Research Institute, Tokai-mura, Naka-gun, Ibaraki-ken, 319-11, Japan.

編集兼発行　日本原子力研究所
印　　刷　いばらき印刷㈱

Energy Transfer and Thermal Conductivity through Inert Matrix and Nuclear Fuel Analogous Materials

Claude DEGUELDRE*, Masahide TAKANO, Toshihiko OHMICHI+
Kousaku FUKUDA, Peter HEIMGARTNER* and Thomas GRABER*

Department of Chemistry and Fuel Research
Tokai Research Establishment
Japan Atomic Energy Research Institute
Tokai-mura, Naka-gun, Ibaraki-ken

(Received October 28, 1997)

Thermal conductivity of zirconia based inert matrix and analogous fuel materials were measured and modelled. Measurements were performed using the laser flash method and systematically applied for binary and ternary zirconia - yttria - erbia as well as quaternary systems including thoria or ceria. Measurements were carried out from room temperature to 1250 K. Thermal conductivity was also modelled taking into account the dopant effect on the lattice parameter of the cubic solid solution, the oxygen vacancy size and their concentration. Experimental and modelled lattice parameter values are compared prior to full justification of the results. In the temperature range from 300 to 950 K, the thermal conductivity of the single phase solid solution with yttria, erbia and ceria as analogous fuel material is about 2 $W \cdot m^{-1}K^{-1}$. Energy transfer in these materials is discussed on the basis of both photonic and phononic conductivities.

Keywords: Energy Transfer, Thermal Conductivity, Laser Flash Method, Inert Matrix, Analogous Fuel Materials, Zirconia, Yttria, Erbia, Thoria, Ceria

---

+ Excess Plutonium Disposition Fuel Research and Development Team

* Paul Scherrer Institute, LWV, 5232 Villigen-PSI, Switzerland

イナートマトリクスおよび模擬燃料材中のエネルギー輸送と熱伝導率

日本原子力研究所東海研究所燃料研究部
Claude DEGUELDRE* ・高野　公秀・大道　敏彦+ ・福田　幸朔
Peter HEIMGARTNER*・Thomas GRABER*

(1997年10月28日受理)

ジルコニアベースのイナートマトリクスおよび模擬燃料材の熱伝導率をレーザーフラッシュ法により測定し、モデル化した。測定対象は、イットリアとエルビアの一方もしくは両方を含む二元系および三元系、さらにトリアもしくはセリアを加えた四元系とした。測定温度範囲は室温から1250Kとした。添加物による立方晶固溶体の格子定数への影響、および酸素原子空孔の大きさと密度を考慮に入れて、熱伝導率をモデル化した。モデル化した結果の妥当性を最終的に検討する前に、実験により得られた格子定数の値と、モデルから得られた格子定数の値を比較検討した。300Kから950Kの温度範囲において、ジルコニアとイットリア、エルビアおよびセリアとの各固溶体の熱伝導率は、約2 $W \cdot m^{-1} \cdot K^{-1}$であった。これらの物質中のエネルギー輸送について、フォトン伝導とフォノン伝導に基づいて検討した。

東海研究所：〒319－11　茨城県那珂郡東海村白方白根2－4
+ 安定化プルトニウム燃料・燃焼法研究特別チーム
* ポールシェラー研究所、スイス

Contents

目　　次

1. Introduction

Recent work has demonstrated the feasibility for burning the excess plutonium by employing a U-free fuel[1),2)]. For this purpose, the fuel material should be composed of inert - fissile - absorbent material components. Stabilised zirconia (ZrO_2 - $YO_{1.5}$) was identified suitable as inert fuel component. A rare earth oxide may be added as absorbent or burnable poison component. Erbium oxide was selected by Degueldre et al., while gadolinium oxide was chosen by Nitani et al. The advantage of erbium in a single phase zirconia based material is that it may contribute to stabilize the solid solution[3)]. These inert matrix components are selected to dissolve the actinide oxide. Here CeO_2 or ThO_2 are taken as an analogous compound of PuO_2. In this study, the phases composed of zirconia, yttria and erbia are called the inert matrix material and those doped with ThO_2 or CeO_2 are called simulated fuel.

To be an efficient fuel, the material must allow an energy transfer through the fuel bulk toward the reactor coolant as large as possible. With advanced inert matrix material, fission energy is not only transferred from the fuel to the coolant by heat transport (as in the traditional UO_2). In addition to this phononic component, one photonic fraction of energy must also be taken into account[4)]. This is due to the fact that the zirconia based material is semi-transparent compared to UO_2 which is black or opaque for a wide range of wavelength ranging from UV to IR[5)].

This paper clarifies how energy may be transferred in zirconia based ceramic and allows to better understand the operational and transient behaviour of a possible inert matrix nuclear fuel.

2. Theoretical background

A fission product recoil yields a thermal spike of the order of 3000 K over a 10 nm range and for a period of the order of 10^{-11} s [6),7)]. The maximum wavelength λ_{max} [m] of the emitted photons associated to this energy spike and material temperature T [K] would be given by:

$$\lambda_{max} \cdot T = 2.898 \times 10^{-3} \quad m \cdot K \tag{1}$$

if the black body theory[8)] can be applied to this system. Clearly, at 5000 K the maximum light emitted is in the visible with λ_{max} around 580 nm and at 1000 K the maximum is 2900 nm. Consequently, radiance in the semi-transparent inert matrix nuclear fuel may not be negligible compared to other energy transfers. However, phononic conversion must take place later when the zone affected by recoil cool down.

The basic energy transfer concept, coupled with phenomenological approaches are used to account for the complement of both phononic and photonic transfers. The effective energy transfer is thus the sum of a phononic heat conductivity component κ_{phn} [$W \cdot m^{-1} \cdot K^{-1}$] and a photonic radiative component κ_{phi}. [$W \cdot m^{-1} \cdot K^{-1}$]. The equation of the energy transfer or effective conductivity κ_{eff} [$W \cdot m^{-1} \cdot K^{-1}$] is simply given by the sum of the two components[9)] as:

1. Introduction

Recent work has demonstrated the feasibility for burning the excess plutonium by employing a U-free fuel[1)2)]. For this purpose, the fuel material should be composed of inert - fissile - absorbent material components. Stabilised zirconia (ZrO_2 - $YO_{1.5}$) was identified suitable as inert fuel component. A rare earth oxide may be added as absorbent or burnable poison component. Erbium oxide was selected by Degueldre et al., while gadolinium oxide was chosen by Nitani et al. The advantage of erbium in a single phase zirconia based material is that it may contribute to stabilize the solid solution[3)]. These inert matrix components are selected to dissolve the actinide oxide. Here CeO_2 or ThO_2 are taken as an analogous compound of PuO_2. In this study, the phases composed of zirconia, yttria and erbia are called the inert matrix material and those doped with ThO_2 or CeO_2 are called simulated fuel.

To be an efficient fuel, the material must allow an energy transfer through the fuel bulk toward the reactor coolant as large as possible. With advanced inert matrix material, fission energy is not only transferred from the fuel to the coolant by heat transport (as in the traditional UO_2). In addition to this phononic component, one photonic fraction of energy must also be taken into account[4)]. This is due to the fact that the zirconia based material is semi-transparent compared to UO_2 which is black or opaque for a wide range of wavelength ranging from UV to IR[5)].

This paper clarifies how energy may be transferred in zirconia based ceramic and allows to better understand the operational and transient behaviour of a possible inert matrix nuclear fuel.

2. Theoretical background

A fission product recoil yields a thermal spike of the order of 3000 K over a 10 nm range and for a period of the order of 10^{-11} s [6),7)]. The maximum wavelength λ_{max} [m] of the emitted photons associated to this energy spike and material temperature T [K] would be given by:

$$\lambda_{max} \cdot T = 2.898 \times 10^{-3} \quad m \cdot K \tag{1}$$

if the black body theory[8)] can be applied to this system. Clearly, at 5000 K the maximum light emitted is in the visible with λ_{max} around 580 nm and at 1000 K the maximum is 2900 nm. Consequently, radiance in the semi-transparent inert matrix nuclear fuel may not be negligible compared to other energy transfers. However, phononic conversion must take place later when the zone affected by recoil cool down.

The basic energy transfer concept, coupled with phenomenological approaches are used to account for the complement of both phononic and photonic transfers. The effective energy transfer is thus the sum of a phononic heat conductivity component κ_{phn} [$W \cdot m^{-1} \cdot K^{-1}$] and a photonic radiative component κ_{phi}. [$W \cdot m^{-1} \cdot K^{-1}$]. The equation of the energy transfer or effective conductivity κ_{eff} [$W \cdot m^{-1} \cdot K^{-1}$] is simply given by the sum of the two components[9)] as:

$$\kappa_{eff} = \kappa_{phn} + \kappa_{phi} \tag{2}$$

The phononic conductivity may be estimated from the classical formula:

$$\kappa_{phn} = \frac{1}{3} \cdot \rho \cdot c_V \cdot \bar{v} \cdot \bar{l} \tag{3}$$

with

$$\bar{v} = \frac{2 \cdot \pi \cdot k \cdot T_D}{h} \cdot \left(\frac{V_O}{6 \cdot \pi^2} \right)^{1/3} \tag{4}$$

where ρ [kg·m^{-3}] is the density, c_V [J·K^{-1}·kg^{-1}] the specific heat capacity, $\bar{v}$ [m·s^{-1}] the average phonon velocity, $\bar{l}$ [m] the phonon mean free path, T_D the Debye temperature [K], V_o the average molecular volume [m^3] and h Planck's constant [J·s].

The phononic conductivity is currently modelled on the basis of its inverse (resistivity R). Its variation with the temperature (T) may be modelled as:

$$\kappa_{phn}^{-1} = R = A + B \cdot T \tag{5}$$

with according to Ambegaokar[10]:

$$A = \frac{4 \cdot \pi^2 \cdot V_O \cdot T_D}{\bar{v}^2 \cdot h} \cdot \Gamma \tag{6}$$

and Gibby[11] :

$$B = \frac{\gamma^2 \cdot h^3}{3.81 \cdot \overline{M} \cdot \overline{V_O}^{1/3} \cdot (k \cdot T_D)^3} \cdot \tag{7}$$

$\Gamma = \Sigma \Gamma_i$ may be estimated as follow[11),12)]:

$$\Gamma_i = \frac{x_i}{12} \left[\left(\frac{M_i - \overline{M}}{\overline{M}} \right)^2 + \varepsilon \cdot \left(\frac{r_i - \bar{r}}{\bar{r}} \right)^2 \right]. \tag{8}$$

For the materials of interest in this study, i.e. for binary, ternary or quaternary mixtures $M_{1-y-z-u}M'_yM''_zM'''_uO_{2-x}$ with a matrix material M and the dopants M', M'' and M''' (for example for M and M''' tetravalent and for M' and M'' trivalents $2 \cdot x = y + z$). In equation (7) and (8), γ is the Grüneisen constant, k the Boltzmann's constant, x_i the molar fraction of the component i, M_i its mass and r_i its ionic radius. ε is given by $32 \cdot (1+1.6 \cdot \gamma)^2$. The average atom mass ($\overline{M}$) and object radius ($\bar{r}$) are given by:

$$\overline{M} = x_M \cdot M_M + \sum x_{M_i'} \cdot M_{M_i'} + x_O \cdot M_O \tag{9}$$

and

$$\bar{r} = x_M \cdot r_M + \sum x_{M_i'} \cdot r_{M_i'} + x_O \cdot r_O + x_{OV} \cdot r_{OV}, \tag{10}$$

where O and OV stand for oxygen and oxygen vacancy, and $x_M + \Sigma x_{M'} + x_O + x_{OV} = 1$.

For phase heterogeneous mixtures, the values of the phononic conductivity becomes much lower than that dictated by this physical law. Its estimation remains therefore subject to hypotheses; it is also linked to the accuracy of the selected values of the parameters.

Because its theoretical approach is still difficult to apply to real phases, the phononic or thermal conductivity must be derived from the experimental thermal diffusivity, and it may be obtained by using the equation:

$$\kappa_{phn} = D \cdot c_p \cdot \rho , \tag{11}$$

where κ_{phn} is the thermal conductivity [$W \cdot m^{-1} \cdot K^{-1}$], D the thermal diffusivity [$m^2 \cdot s^{-1}$] corrected from the porosity, c_p the specific heat capacity [$J \cdot kg^{-1} \cdot K^{-1}$], and ρ the bulk density of the material [$kg \cdot m^{-3}$].

On the other hand the photonic conductivity component may be estimated and for a mono-crystal of infinite thickness, it is given by [13]:

$$\kappa_{pht} = \frac{16 \cdot \sigma \cdot n^2 \cdot T^3}{3 \cdot a(\lambda)} \tag{12}$$

where σ is the radiation constant: 5.672×10^{-12} $W \cdot m^{-2} \cdot K^{-4}$, $a(\lambda)$ the absorption coefficient of the material [m^{-1}] at the wavelength λ [m], T the absolute temperature [K] and n [-] the breaking index of the material. Now, for phase mixtures $a(\lambda)$ additivity is generally acceptable, except when specific solvent effects affect the additivity. This should not be expected for the solid solution derived from the stabilised zirconia. However, the system supposed to form the suggested fuel is not mono-crystalline but more specifically poly-crystalline in which case each interface may be a source of photonic reflections.

3. Experimental

3.1 Material preparation

The preparation of all zirconia based materials was carried out by the wet route because it was earlier found that it gave the best material based on relative theoretical density[14]. The material was prepared by mixing nitrate solution of each element (Zr, Y, Er, Th or Ce) composing constituents in the final product. Co-precipitation was carried out by adding ammonia under strong stirring. The precipitate was filtered on paper filter and washed 10 times with ultrapure water. The filtered phase was contacted with alcohol and milled utilising a Retch unit with zirconia container and bowls. The wet powder was then dried for 24 hours at 420 K. The dried powder was calcined for 5 hours at 900 K. The calcined powder was milled again utilising the Rech unit with zirconia vessel. The final powder was then pressed at 352 MPa for 10 seconds, and pellets of 11 mm in diameter were obtained. Pelletised samples were then sintered in an oven with a temperature program including a first step at 1500 K for 4 hours followed by a final step of 48 hours at 1900 K.

Because its theoretical approach is still difficult to apply to real phases, the phononic or thermal conductivity must be derived from the experimental thermal diffusivity, and it may be obtained by using the equation:

$$\kappa_{phn} = D \cdot c_p \cdot \rho , \tag{11}$$

where κ_{phn} is the thermal conductivity [$W \cdot m^{-1} \cdot K^{-1}$], D the thermal diffusivity [$m^2 \cdot s^{-1}$] corrected from the porosity, c_p the specific heat capacity [$J \cdot kg^{-1} \cdot K^{-1}$], and ρ the bulk density of the material [$kg \cdot m^{-3}$].

On the other hand the photonic conductivity component may be estimated and for a mono-crystal of infinite thickness, it is given by [13]:

$$\kappa_{pht} = \frac{16 \cdot \sigma \cdot n^2 \cdot T^3}{3 \cdot a(\lambda)} \tag{12}$$

where σ is the radiation constant: 5.672×10^{-12} $W \cdot m^{-2} \cdot K^{-4}$, $a(\lambda)$ the absorption coefficient of the material [m^{-1}] at the wavelength λ [m], T the absolute temperature [K] and n [-] the breaking index of the material. Now, for phase mixtures $a(\lambda)$ additivity is generally acceptable, except when specific solvent effects affect the additivity. This should not be expected for the solid solution derived from the stabilised zirconia. However, the system supposed to form the suggested fuel is not mono-crystalline but more specifically poly-crystalline in which case each interface may be a source of photonic reflections.

3. Experimental

3.1 Material preparation

The preparation of all zirconia based materials was carried out by the wet route because it was earlier found that it gave the best material based on relative theoretical density[14]. The material was prepared by mixing nitrate solution of each element (Zr, Y, Er, Th or Ce) composing constituents in the final product. Co-precipitation was carried out by adding ammonia under strong stirring. The precipitate was filtered on paper filter and washed 10 times with ultrapure water. The filtered phase was contacted with alcohol and milled utilising a Retch unit with zirconia container and bowls. The wet powder was then dried for 24 hours at 420 K. The dried powder was calcined for 5 hours at 900 K. The calcined powder was milled again utilising the Rech unit with zirconia vessel. The final powder was then pressed at 352 MPa for 10 seconds, and pellets of 11 mm in diameter were obtained. Pelletised samples were then sintered in an oven with a temperature program including a first step at 1500 K for 4 hours followed by a final step of 48 hours at 1900 K.

3.2 Sample characterization

The sintered pellets to final relative densities ranging from 92 to 80 %TD. Disk samples of 9.60 ± 0.35 mm in diameter and about 1 mm in thickness were prepared by cutting the original pellets utilising a diamond saw. The density of the material was determined by measuring the sizes (diameter and thickness) and weight utilising a Mettler balance (AG204). Size, weight and densities are given in Table 1. ρ is the theoretical density and ρ_{exp} is the geometrical density of the pellet.

X-ray diffraction (XRD) analysis was carried out on the crushed pellets in order to identify the phases and the lattice parameter. The XRD unit was a Phillips diffractometer PW1710, equipped with a Cu X-ray tube. The samples were analysed after crushing and lattice parameters were measured with a precision ranging from ± 0.001 to 0.0001 nm. The absence of any other phases as the cubic phase was confirmed in the inert matrix and simulated fuel materials.

3.3 Thermal conductivity measurements

Disk samples were preliminary examined and those presenting any heterogeneity, small fissure or hole were discarded. Since the samples are white or slightly coloured, the surface of the disk samples was treated with gold and carbon[15]. Gold was physically vapour deposited on the surface to prevent the sample from transmitting the laser beam through the semi-transparent material. Surface treatment was completed by carbon powder spray on the surface to absorb efficiently the laser beam. The coating is very thin so that its influence on the measured thermal diffusivity is less than 1 %. The thermal diffusivity of the zirconia based disk samples was measured from room temperature to 1250 K by the laser flash method[16]. The measurements were performed in vacuum below 3×10^{-3} Pa.

The sample was heated in an electric furnace to the required temperatures and the sample temperature was measured with a thermocouple near the sample. The method consists in illuminating the front face of the disc with a short laser pulse creating a heat pulse at the surface when the light is adsorbed. The energy of the laser pulse is 6 J which allow locally a temperature increase of the sample surface of some 10 K. The thermal diffusivity D_{exp} is deduced from the thermal transient of the rear face, called thermogram. The temperature rise at the rear surface measured by a In-Sb infrared detector after the front surface of the sample was heated by a ruby laser pulse. The data of the temperature change were analysed using the logarithmic method[17]. The unit for thermal diffusivity was tested using a stainless-steel sample (SUS304) as standard. The experimental uncertainty was less than 3%.

4. Results

4.1 Effect of the sample preparation

As mentioned earlier, the thermal conductivity is measured with double coated samples in order to translate the photonic pulse of the laser flash in a thermal pulse. For regular measurements, semi-transparent samples are coated on both faces so that the light pulse is transformed in a thermal impulse on the incident surface, the transmitted thermal signal is then detected on the rear surface. Figure 1 shows a comparison of the signal obtained for two type of sample: the first one with both sample sides coated and the second one with the back side coated only. The uncoated signal is not presented because it would be null for a thermometer and would be the laser flash light in the detector. Figure 1 presents the phenomenological complement of energy transfer processes and shows that both phononic and photonic transfers may be registered separately for the specimen.

It must be noted that for a UO_2 sample the uncoated and coated thermogram are the same because the material is black in the visible, near infrared and infrared spectral area.

4.2 Effect of material composition at room temperature

The relative density of the material is derived from the experimental density obtained by measuring sizes and weight of the disks or pellets and from the theoretical density obtained from the atomic weight and lattice parameter. The conductivity results for the studied samples (see Table 1) are given in Table 2 for room temperature measurements. All specimen examined were carbon coated on both faces and the experimental diffusivity D_{exp} corrected from the relative density $\rho_{exp}\cdot\rho^{-1}$ to obtain the material thermal diffusivity $D = D_{exp}\cdot\rho\cdot\rho_{exp}^{-1}$. The effect of component mixing was first investigated at room temperature.

For the binary mixture $Zr_{1-y}Y_yO_{2-x}$ or $Zr_{1-z}Er_zO_{2-x}$, the thermal conductivity changes in a comprehensive way. It decreases when the dopant concentration increases. Results are given in Table 2. For ternary systems $Zr_{1-y-z}Y_yEr_zO_{2-x}$ and for the investigated concentrations, the thermal conductivity was nearly 2 $W\cdot m^{-1}\cdot K^{-1}$. For quaternary systems $Zr_{1-y-z-u}Y_yEr_zCe_uO_{2-x}$ and for the investigated concentrations, the thermal conductivity was a bit larger than 2 $W\cdot m^{-1}\cdot K^{-1}$ and is slightly increasing with the Ce concentration. For Th doped sample, the conductivity is, however, reduced.

4.3 Effect of temperature

The effect of temperature was studied from room temperature to 1250 K. The conductivity was rather constant at temperatures range below 950 K (Table 3) for a ternary system $Zr_{1-y-z}Y_yEr_zO_{2-x}$. However, above this temperature, it increased systematically. This increase in conductivity was later identified to be due to the carbon coating sublimation and direct photonic transfer. This fully

demonstrates that the conductivity of the real sample may effectively be larger than that measured for phononic transport.

The measured thermal diffusivities of two quaternary samples, Zr10Y5Er10Ce and Zr10Y5Er10Th, are shown in Figure 2 **a** and **b**. Their thermal conductivities are listed in Table 4 and 5.

5. Discussion

5.1 Modelling

In order to understand the measured data, conductivity modelling was performed and the experimental data were compared with the calculated one utilising classical models. Ohmichi[19] reviewed the calculation (equation 3 and 4) for stabilised zirconia considering its Debye temperature to be 800 K and the phonon pathway of 0.3 nm. Calculation of phonon velocity of 8×10^3 m·s^{-1} may yield a thermal conductivity of 2 W·m^{-1}·K^{-1}.

To calculate the thermal resistivity utilising equations (5-8), a defined evaluation of the lattice parameter or of the cation-anion distance is required. This is done by analysing the ionic radii for the species considered in this study. This allows to estimate the radius of the oxygen vacancy. The basic data are reported in Table 6. The lattice parameter (a) or the cation-anion distance ($d = a\cdot4\cdot(3)^{-0.5}$) of the cubic zirconia samples was calculated as a function of the rare earth dopant.

For $Zr_{1-y-z-u}Y_yEr_zCe_uO_{2-x}$ with $2x = (y+z)$ given from the charge balance relation for Zr^{4+}, Y^{3+}, Er^{3+}, Ce^{4+} and O^{2-}, the cation (i) -anion (j) distance d in the solid solution is expressed as $d = \Sigma x_i \cdot r_i + \Sigma x_j \cdot r_j$ (with $\Sigma x_i + \Sigma x_j = 1$) or:

$$d = x_{Zr}\cdot r_{Zr} + x_Y\cdot(r_Y - r_{Zr}) + x_{Er}\cdot(r_{Er} - r_{Zr}) + x_{Ce}(r_{Ce} - r_{Zr}) + x_O\cdot r_O + x_{OV}\cdot(r_{OV} - r_O) \quad (13)$$

With $\beta = \Sigma x_i(\Delta r_i \cdot \Delta x^{-1})$ and according to the relation:

$$\frac{\Delta r_i}{\Delta x_i} = \left(\frac{\Delta r_i}{\Delta(CN)}\right)\cdot\left(\frac{\Delta(CN)}{\Delta x_i}\right) \quad (14)$$

The value of $(\Delta r_i \cdot \Delta x^{-1})$ is 24 pm for r_{Zr}, r_Y and r_{Er} and 20 pm for r_{Ce}. Calculation tests were performed with the ion radius values given by Shanon[20] (see Table 6). For O^{2-}, 136.4 pm was used as the best fit with the lattice parameter of cubic zirconia a = 500.9 pm (d= 220.4 pm). Figure 3a shows the correlation study of d_{exp} - d_{cal} - $\beta\cdot x$ again $2\cdot x$ for the solid solution not-containing Ce. d_{exp} is the experimental value obtained by XRD and d_{cal} is calculated utilising equation (13). A straight relation exists between both values. From the slope, the value of r_{OV} is derived for the stabilised zirconia sample non-doped with ceria giving its value of 160 pm. In the zirconia-yttria-erbia system yttria and erbia are comparable for their stabilization role of the material. Figure 3b is similarly obtained for the solid solutions containing ceria (about 10 atom %). In this case, the value of r_{OV} obtained is 172 pm.

Using equations (5-8) it is then possible to calculate the phononic conductivity of the zirconia based material.

demonstrates that the conductivity of the real sample may effectively be larger than that measured for phononic transport.

The measured thermal diffusivities of two quaternary samples, Zr10Y5Er10Ce and Zr10Y5Er10Th, are shown in Figure 2 **a** and **b**. Their thermal conductivities are listed in Table 4 and 5.

5. Discussion

5.1 Modelling

In order to understand the measured data, conductivity modelling was performed and the experimental data were compared with the calculated one utilising classical models. Ohmichi[19] reviewed the calculation (equation 3 and 4) for stabilised zirconia considering its Debye temperature to be 800 K and the phonon pathway of 0.3 nm. Calculation of phonon velocity of 8×10^3 m·s^{-1} may yield a thermal conductivity of 2 W·m^{-1}·K^{-1}.

To calculate the thermal resistivity utilising equations (5-8), a defined evaluation of the lattice parameter or of the cation-anion distance is required. This is done by analysing the ionic radii for the species considered in this study. This allows to estimate the radius of the oxygen vacancy. The basic data are reported in Table 6. The lattice parameter (a) or the cation-anion distance ($d = a\cdot4\cdot(3)^{-0.5}$) of the cubic zirconia samples was calculated as a function of the rare earth dopant.

For $Zr_{1-y-z-u}Y_yEr_zCe_uO_{2-x}$ with $2x = (y+z)$ given from the charge balance relation for Zr^{4+}, Y^{3+}, Er^{3+}, Ce^{4+} and O^{2-}, the cation (i) -anion (j) distance d in the solid solution is expressed as $d = \Sigma x_i\cdot r_i + \Sigma x_j\cdot r_j$ (with $\Sigma x_i+\Sigma x_j = 1$) or:

$$d = x_{Zr}\cdot r_{Zr} + x_Y\cdot(r_Y - r_{Zr}) + x_{Er}\cdot(r_{Er} - r_{Zr}) + x_{Ce}\cdot(r_{Ce} - r_{Zr}) + x_O\cdot r_O + x_{OV}\cdot(r_{OV} - r_O) \quad (13)$$

With $\beta=\Sigma x_i(\Delta r_i\cdot\Delta x^{-1})$ and according to the relation:

$$\frac{\Delta r_i}{\Delta x_i} = \left(\frac{\Delta r_i}{\Delta(CN)}\right)\cdot\left(\frac{\Delta(CN)}{\Delta x_i}\right) \quad (14)$$

The value of $(\Delta r_i\cdot\Delta x^{-1})$ is 24 pm for r_{Zr}, r_Y and r_{Er} and 20 pm for r_{Ce}. Calculation tests were performed with the ion radius values given by Shanon[20] (see Table 6). For O^{2-}, 136.4 pm was used as the best fit with the lattice parameter of cubic zirconia a = 500.9 pm (d= 220.4 pm). Figure 3a shows the correlation study of $d_{exp} - d_{cal} - \beta\cdot x$ again $2\cdot x$ for the solid solution not-containing Ce. d_{exp} is the experimental value obtained by XRD and d_{cal} is calculated utilising equation (13). A straight relation exists between both values. From the slope, the value of r_{OV} is derived for the stabilised zirconia sample non-doped with ceria giving its value of 160 pm. In the zirconia-yttria-erbia system yttria and erbia are comparable for their stabilization role of the material. Figure 3b is similarly obtained for the solid solutions containing ceria (about 10 atom %). In this case, the value of r_{OV} obtained is 172 pm.

Using equations (5-8) it is then possible to calculate the phononic conductivity of the zirconia based material.

5.2 Effect of component mixing at a given temperature

Thermal conductivity experimental results obtained for binary, ternary and quaternary systems ($Zr_{1-y-z-u}Y_yEr_zCe_uO_{2-x}$) are presented in Figure 4 together with values calculated using the adapted model predictions. Calculations were performed using equations derived from the model presented earlier on the resistivity (equations 5, 6 and 8). The equation of the resistivity is:

$$R_i = \left(\kappa_{phn} - \kappa_{phn(ZrO_2)}\right)^{-1} \tag{15}$$

with $R_i = \pi^{5/3} \cdot V_O^{2/3} \cdot 36^{-1/3} \cdot k^{-1} \cdot \Delta\Gamma$ and:

$$\Delta\Gamma = \left[\left(\frac{x_M \cdot M_M^2 + \sum x_{M'} \cdot M_{M'}^2}{\overline{M}^2} - \frac{3 \cdot M_M^2}{(M_M + 2 \cdot M_O)^2}\right) + \left(\frac{x_O \cdot M_O^2}{\overline{M}^2} - \frac{6 \cdot M_O^2}{(M_M + 2 \cdot M_O)^2}\right)\right]$$
$$+\varepsilon \cdot \left[\left(\frac{x_M \cdot r_M^2 + \sum x_{M'} \cdot r_{M'}^2}{\overline{r}^2} - \frac{3 \cdot r_M^2}{(r_M + 2 \cdot r_O)^2}\right) + \left(\frac{x_O \cdot r_O^2 + x_{OV} \cdot r_{OV}^2}{\overline{r}^2} - \frac{6 \cdot r_O^2}{(r_M + 2 \cdot r_O)^2}\right)\right] \tag{16}$$

R_i was calculated in the case of the sample non doped with Ce considering r_{OV} = 160 pm and ε = 200 and in the case of the Ce doped samples with r_{OV} = 172 pm and ε = 250. In the calculation, the value 1.6427 [W^{-1}·m·K] was used for $\pi^{5/3} \cdot V_0^{2/3} \cdot (36)^{1/3} \cdot k^{-1}$. The results for both doped and non-doped samples with Ce are given in Figure 4. As seen in the figure the conductivity values for the specimens Zr10Y5Er and Zr10Y7Er15Ce are more difficult to be fitted.

The modelling is based on the effect of ion masses and radii, as well as on the presence of vacancies. Clearly according to equation (16) the mass effect has less impact on the thermal conductivity than the ion size effect, indicating that this is due to the rather high value of ε. The addition of yttria and erbia increases the proportion of vacancies in the solid solution and decreases consequently the thermal conductivity. On the other hand, addition of ceria into the solid solution should increase slightly the thermal conductivity because the cation-anion distance increases consequently. However, the size of the vacancies increases when adding ceria.

In this study the presence of the 1-2% hafnium as impurity in the zirconium is not considered. Since its ion size is comparable to that of zirconia, its impact on Γ is not significant (equations 6 & 8).

5.3 Results as a function of temperature

For all the samples studied as a function of temperature, it was noted that the conductivity was rather invariant with the temperature. B in equation (5) is found experimentally to be about zero. This is due to the fact that in equation (7) Debye temperature is rather large (800 K for ZrO_2 and 242 K for UO_2) and the Grüneisen constant γ is smaller than 1 (e.g. 0.9 for ZrO_2 and 1.6 for UO_2). In these conditions, B for ZrO_2 is much smaller than that for UO_2. For example, Gibby[11] found for UO_2 2.29×10^{-4} m·W^{-1}. The value of B for ZrO_2 should at least be one order of magnitude smaller than that for UO_2. Consequently,

the resistivity and therefore the conductivity of ZrO_2 is expected to be constant and non-temperature dependent. Figure 5 presents this result for the inert matrix material.

In this work, results are not corrected from the thermal expansion coefficient of zirconia (8×10^{-6} K^{-1}). The correction on the conductivity would be small over the experimental temperature range (e.g. 0.6% for 400 K) and negligible with regard to the 10% accepted in this study.

5.4 Estimation for a plutonium doped sample

The results and the modelling show clearly that the thermal conductivity decreases with addition of yttria or erbia and that its value may increase with addition of ceria. The same behaviour would be expected with addition of plutonia. Addition of ceria or plutonia into the solid solution should increase the thermal conductivity according to the modelling.

5.5 Action of the disc coating and analogy thermal spike - laser flash

Clearly the nuclear thermal spike would interact in a similar way into the material as the laser pulse on the uncoated disk. If not transformed by the carbon coating, a laser pulse or the photons emitted by a thermal spike will be transferred through the fuel material from its local impact to all directions. This is not the case with UO_2 because this material is not semi-transparent at the mm scale. The latter material transforms then all photonic transfer in phononic conduction. Zirconia if pure is semi transparent and allows energy transfer by photonic facilitated mechanism. This would not be the case at low temperature thermal spike and with doped or dirty (e.g. crude coated zirconia as result of cladding oxidation) because impurities such as iron in crude coatings also absorb strongly in the Vis- NIR region substituting the photonic in phononic transport.

Potential impact of the photonic conductivity has to be taken into account. Effective energy transfer is evaluated considering first $\kappa_{eff} = \kappa_{phn}$ only, and secondly considering $\kappa_{eff} = \kappa_{phn} + \kappa_{phi}$. For zirconia, n is 2.2 and $a(\lambda)$ is very low (e.g. 10^{-3} to 10^{-2} m^{-1}) so κ_{phi} calculated with equation (12) ranges from 18 to 1.8 $W\cdot m^{-1}\cdot K^{-1}$. In addition this value increases very rapidly with temperature.

Absorption coefficients of the main components may be estimated from the infrared spectra literature. Zirconia is rather transparent in a wide spectral area. Main peaks are around 15 to 30 μm[21),22)]. IR spectra of other materials composing the inert matrix or of interest for this study are shown in Figure 6. It must be noted that while UO_2 is black and opaque in a large spectral area, the other materials are rather transparent. Presently the degree of transparency is linked to the grain size distribution of the material.

It is difficult to anticipate the changes of the optical properties of the inert matrix fuel during irradiation in the reactor because the formation of fission product ions will modify the photonic absorption properties of the material and because of irradiation induced structural and electronic modifications in the fuel materials. Therefore, the real thermal conductivity in the fuel material is expected to be comprised between the two limiting cases that given by κ_{phn} only, and $\kappa_{phn}+\kappa_{phi}$. However,

the concentration of fission products will never be larger than 1 at% in the spent fuels, and the irradiation damages generated will currently be repaired by annealing of the zirconia based material.

6. Conclusion

The main mechanisms describing the energy transfer in the studied zirconia based materials have been identified. The thermal conductivities of the investigated inert matrix and simulated fuel materials were found to be between 2.0 and 2.6 $W \cdot m^{-1} \cdot K^{-1}$ and they were rather independent of the temperature. The yttria and/or erbia presence decreases the thermal conductivity. However, ceria addition may slightly increase the conductivity when the material forms a solid solution. Presence of heterogeneity or excess of trivalent rare earth dopant concentration may decrease the conductivity by increasing the oxygen vacancy concentration. Photonic conductivity is, however, expected to contribute to a proportion of the energy transfer in these materials, as indicated by the measurement. The effect of yttria and erbia addition can be best modelled using equation (15) and (16) with $r_{ov} = 160$ pm and $\varepsilon = 200$.

Acknowledgements

G. Ledergerber head of the Advanced Nuclear Fuel program at PSI and Dr T. Muromura head of the PROFIT team at JAERI are thanked for their support and direct interest in this work. K. Minato and T. Shiratori at JAERI as well as M. Pouchon, J. Dayer and Y. Mai at PSI are thanked for their technical support.

the concentration of fission products will never be larger than 1 at% in the spent fuels, and the irradiation damages generated will currently be repaired by annealing of the zirconia based material.

6. Conclusion

The main mechanisms describing the energy transfer in the studied zirconia based materials have been identified. The thermal conductivities of the investigated inert matrix and simulated fuel materials were found to be between 2.0 and 2.6 $W \cdot m^{-1} \cdot K^{-1}$ and they were rather independent of the temperature. The yttria and/or erbia presence decreases the thermal conductivity. However, ceria addition may slightly increase the conductivity when the material forms a solid solution. Presence of heterogeneity or excess of trivalent rare earth dopant concentration may decrease the conductivity by increasing the oxygen vacancy concentration. Photonic conductivity is, however, expected to contribute to a proportion of the energy transfer in these materials, as indicated by the measurement. The effect of yttria and erbia addition can be best modelled using equation (15) and (16) with $r_{ov} = 160$ pm and $\varepsilon = 200$.

Acknowledgements

G. Ledergerber head of the Advanced Nuclear Fuel program at PSI and Dr T. Muromura head of the PROFIT team at JAERI are thanked for their support and direct interest in this work. K. Minato and T. Shiratori at JAERI as well as M. Pouchon, J. Dayer and Y. Mai at PSI are thanked for their technical support.

the concentration of fission products will never be larger than 1 at% in the spent fuels, and the irradiation damages generated will currently be repaired by annealing of the zirconia based material.

6. Conclusion

The main mechanisms describing the energy transfer in the studied zirconia based materials have been identified. The thermal conductivities of the investigated inert matrix and simulated fuel materials were found to be between 2.0 and 2.6 $W \cdot m^{-1} \cdot K^{-1}$ and they were rather independent of the temperature. The yttria and/or erbia presence decreases the thermal conductivity. However, ceria addition may slightly increase the conductivity when the material forms a solid solution. Presence of heterogeneity or excess of trivalent rare earth dopant concentration may decrease the conductivity by increasing the oxygen vacancy concentration. Photonic conductivity is, however, expected to contribute to a proportion of the energy transfer in these materials, as indicated by the measurement. The effect of yttria and erbia addition can be best modelled using equation (15) and (16) with $r_{ov} = 160$ pm and $\varepsilon = 200$.

Acknowledgements

G. Ledergerber head of the Advanced Nuclear Fuel program at PSI and Dr T. Muromura head of the PROFIT team at JAERI are thanked for their support and direct interest in this work. K. Minato and T. Shiratori at JAERI as well as M. Pouchon, J. Dayer and Y. Mai at PSI are thanked for their technical support.

References

1) Degueldre C., Kasemeyer U., Botta F. and Ledergerber G. : "Mat. Res. Soc. Symp. Proc.", 412, 15 (1996).
2) Nitani N., Akie H., Takano H., Ohmichi T. and Muromura T. : "Proc. PSI workshop on Advanced Fuel Cycles", PSI, Villigen, Switzerland Nov. 1995, 118 (1995).
3) Yokokawa H., Sakai N., Kawada T. and Dokiya M. : J. Austral. Ceram. Soc. 28(1), 81 (1992).
4) Incropera F. and DeWitt D. : "Fondamental of heat transfer", J. Wiley & Sons, New York (1981).
5) Handbook
6) Izui K. : J. Phys. Soc. Jap. 20(6), 67 (1965).
7) Waligorski M., Hamm R. and Katz R. : Nucl. Tracks Radiat. Meas. 11, 309 (1986).
8) Planck M. : "The theory of heat radiation", Dover Publication, New York (1959).
9) Lechner T. : "Bestimmung der Temperaturleitfähigkeit semitransparenter Materialien mit dem Laser-impulsverfahren. Messungen an kristallinem und gesintertem Al_2O_3 und MgO", Fortschritt-Bericht, Reihe 19, Nr. 90, VDI Verlag GmbH Düsseldorf, Germany (1996).
10) Ambegaokar V. : Phys. Rev. 114, 488 (1959).
11) Gibby R. : J. Nucl. Mat. 38, 163 (1971).
12) Abeles B. : Phys. Rev. 131, 1906 (1963).
13) Kingery W. : "Introduction to ceramics", John Wiley & Sons, New York (1960).
14) Degueldre C., Heimgartner P., Ledergerber G., Sasajima N., Hojou K., Muramura T., Wang L., Gong W. and Ewing R. : "Mat. Res. Soc. Symp. Proc.", 439, 625 (1997).
15) Minato K., Takano M., Fukuda K., Sato S. and Ohashi H. : J. Alloys Compon. 255,18 (1997).
16) Parker W., Jenkins R., Butler C. and Abbott. G. : J. Appl. Phys. 32, 1679 (1961).
17) James H. : J. Appl. Phys. 51, 4666 (1980).
18) Touloukian Y. and Buyco E. : "Thermophysical properties of matter Vol 5. Non-metallic solids", IFI plenum, New York (1970).
19) Ohmichi T. : JAERI-Review 96-008, "Assessment of swelling of rock-like fuel by irradiation", (1996).
20) Shannon R. and Prewitt C. : Acta Cryst. B25, 925 (1969).
21) McDevitt N. and Baun W. : J. Am. Ceram. Soc. 47(12), 622 (1964).
22) Phillippi C. and Mazdiyasni K. : J. Am. Ceram. Soc. 54(5), 254 (1971).

Table 1 Sample density, size, weight and relative density

Conditions: Pellet press CAUO-10, matrix diameter: 11.6 mm, lubrification with stearic acid, pressing time: 10 s, pressure on the pellet 352 MPa, Sintering oven: Güller, sintering atmosphere: air, sintering rate 5 K·min^{-1}, 1500 K for 4 h, 1900 K for 48 h. The precision on $\rho_{exp}\cdot\rho^{-1}$ is about 4%. Note: in ZrnY, n stands for the Y concentration in at%.

Sample	ρ/kg·m^{-3}	d/m	h/m	m/kg	$\rho_{exp}\cdot\rho^{-1}$/%
Zr	5.89 10^{-3}	9.36 10^{-3}	8.5 10^{-4}	2.86 10^{-4}	83
Zr10Y	5.80 10^{-3}	9.40 10^{-3}	8.4 10^{-4}	3.02 10^{-4}	88
Zr20Y	5.70 10^{-3}	9.83 10^{-3}	7.8 10^{-4}	2.72 10^{-4}	82
Zr30Y	5.61 10^{-3}	9.75 10^{-3}	8.3 10^{-4}	2.97 10^{-4}	83
Zr10Er	6.18 10^{-3}	9.70 10^{-3}	8.5 10^{-4}	3.25 10^{-4}	81
Zr10Y5Er	5.94 10^{-3}	9.50 10^{-3}	8.3 10^{-4}	3.23 10^{-4}	92
Zr20Y5Er	5.85 10^{-3}	9.84 10^{-3}	8.5 10^{-4}	3.26 10^{-4}	86
Zr15Y5Er10Ce	6.03 10^{-3}	9.60 10^{-3}	8.2 10^{-4}	3.12 10^{-4}	89
Zr15Y5Er10Th	6.23 10^{-3}	9.95 10^{-3}	8.3 10^{-4}	3.22 10^{-4}	80
Zr10Y7Er15Ce	6.20 10^{-3}	9.25 10^{-3}	8.6 10^{-4}	3.01 10^{-4}	83

Table 2 Thermophysical characteristic of the zirconia based samples, effect of the composition

Conditions: temperature RT (293 K), $c_p=\Sigma x_i\cdot c_{pi}$ with c_{pi} data from Touloukian[18] with c_{pZrO2} = 4.509, $c_{pYO1.5}$ = 4.522, $c_{pErO1.5}$ = 2.81, c_{pCeO2} = 3.55, c_{pThO2} = 2.32×10^{+2} J·kg^{-1}·K^{-1}, respectively. Note : in the system $Zr_{1-y-z-u}Y_yEr_zCe_uO_{2-x}$, only 1 phase is observed for $y+z > 0.10$. Precision on D : 10% and on κ_{phn} also about 10%.

Sample	D/m^2·s^{-1}	ρ/kg·m^{-3}	c_p/J·kg^{-1}·K^{-1}	κ_{phn}/W·m^{-1}·K^{-1}
Zr	10.55 10^{-7}	5.89 10^{+3}	4.509 10^{+2}	2.80
Zr10Y	9.20 10^{-7}	5.80 10^{+3}	4.510 10^{+2}	2.41
Zr20Y	10.21 10^{-7}	5.70 10^{+3}	4.511 10^{+2}	2.40
Zr30Y	8.41 10^{-7}	5.61 10^{+3}	4.513 10^{+2}	2.13
Zr10Er	9.50 10^{-7}	6.18 10^{+3}	4.259 10^{+2}	2.50
Zr10Y5Er	7.86 10^{-7}	5.94 10^{+3}	4.381 10^{+2}	2.04
Zr20Y5Er	8.82 10^{-7}	5.85 10^{+3}	4.381 10^{+2}	2.26
Zr15Y5Er10Ce	8.60 10^{-7}	6.03 10^{+3}	4.259 10^{+2}	2.20
Zr15Y5Er10Th	7.07 10^{-7}	6.23 10^{+3}	3.978 10^{+2}	1.75
Zr10Y7Er15Ce	9.17 10^{-7}	6.20 10^{+3}	4.156 10^{+2}	2.36

Table 3 Thermophysical characteristic of the Zr10Y5Er sample

Conditions: $d = 9.50\times10^{-3}$ m, $h = 8.3\times10^{-4}$ m, $m = 3.23\times10^{-4}$ kg, c_p data from Touloukian[18] for pure ZrO_2. Precision : 10%. Note: above 950 K, the carbon coating sublimates and part of the laser pulse passes through the pellet and consequently increasing the apparent conductivity by a photonic component.

T/K	$D/m^2\cdot s^{-1}$	$\rho/kg\cdot m^{-3}$	$c_p/J\cdot kg^{-1}\cdot K^{-1}$	$\kappa_{phn}/W\cdot m^{-1}\cdot K^{-1}$
293	$7.86\ 10^{-7}$	$5.94\ 10^{+3}$	$4.498\ 10^{+2}$	2.10
357	$7.56\ 10^{-7}$	$5.94\ 10^{+3}$	$4.887\ 10^{+2}$	2.20
434	$7.28\ 10^{-7}$	$5.94\ 10^{+3}$	$5.247\ 10^{+2}$	2.27
525	$7.09\ 10^{-7}$	$5.94\ 10^{+3}$	$5.565\ 10^{+2}$	2.34
628	$6.95\ 10^{-7}$	$5.94\ 10^{+3}$	$5.775\ 10^{+2}$	2.38
704	$6.84\ 10^{-7}$	$5.94\ 10^{+3}$	$5.900\ 10^{+2}$	2.40
788	$6.27\ 10^{-7}$	$5.94\ 10^{+3}$	$5.990\ 10^{+2}$	2.42
880	$6.75\ 10^{-7}$	$5.94\ 10^{+3}$	$6.100\ 10^{+2}$	2.47
970	$6.70\ 10^{-7}$	$5.94\ 10^{+3}$	$6.165\ 10^{+2}$	2.45
1065	$6.78\ 10^{-7}$	$5.94\ 10^{+3}$	$6.220\ 10^{+2}$	2.51
1159	$7.52\ 10^{-7}$	$5.94\ 10^{+3}$	$6.275\ 10^{+2}$	2.80
1238	$8.01\ 10^{-7}$	$5.94\ 10^{+3}$	$6.315\ 10^{+2}$	3.00

Table 4 Thermophysical characteristic of the Zr15Y5Er10Ce sample

Condition: Zr15Y5Er10Ce, diameter 9.60 mm, thickness 0.81 mm, weight 312 mg.

T/K	$D/m^2\cdot s^{-1}$	$\rho/kg\cdot m^{-3}$	$c_p/J\cdot kg^{-1}\cdot K^{-1}$	$\kappa_{phn}/W\cdot m^{-1}\cdot K^{-1}$
289	$8.62\ 10^{-7}$	$6.03\ 10^{+3}$	$4.500\ 10^{+2}$	2.34
371	$8.11\ 10^{-7}$	$6.03\ 10^{+3}$	$4.998\ 10^{+2}$	2.45
462	$7.75\ 10^{-7}$	$6.03\ 10^{+3}$	$5.302\ 10^{+2}$	2.48
570	$7.50\ 10^{-7}$	$6.03\ 10^{+3}$	$5.643\ 10^{+2}$	2.55
636	$7.39\ 10^{-7}$	$6.03\ 10^{+3}$	$5.796\ 10^{+2}$	2.58
741	$7.26\ 10^{-7}$	$6.03\ 10^{+3}$	$5.962\ 10^{+2}$	2.61
839	$7.20\ 10^{-7}$	$6.03\ 10^{+3}$	$6.018\ 10^{+2}$	2.61
924	$7.19\ 10^{-7}$	$6.03\ 10^{+3}$	$6.120\ 10^{+2}$	2.65
1015	$7.18\ 10^{-7}$	$6.03\ 10^{+3}$	$6.201\ 10^{+2}$	2.68
1088	$7.32\ 10^{-7}$	$6.03\ 10^{+3}$	$6.234\ 10^{+2}$	2.75

Table 5 Thermophysical characteristic of the Zr15Y5Er10Th sample
Conditions: diameter 9.95 mm, thickness 0.82 mm, weight 322 mg.

T/K	$D/m^2 \cdot s^{-1}$	$\rho/kg \cdot m^{-3}$	$c_p/J \cdot kg^{-1} \cdot K^{-1}$	$\kappa_{phn}/W \cdot m^{-1} \cdot K^{-1}$
289	$7.07\ 10^{-7}$	$6.22\ 10^{+3}$	$4.500\ 10^{+2}$	1.98
372	$6.81\ 10^{-7}$	$6.22\ 10^{+3}$	$5.000\ 10^{+2}$	2.11
450	$6.62\ 10^{-7}$	$6.22\ 10^{+3}$	$5.111\ 10^{+2}$	2.11
567	$6.45\ 10^{-7}$	$6.22\ 10^{+3}$	$5.630\ 10^{+2}$	2.25
639	$6.37\ 10^{-7}$	$6.22\ 10^{+3}$	$5.805\ 10^{+2}$	2.30
729	$6.29\ 10^{-7}$	$6.22\ 10^{+3}$	$5.931\ 10^{+2}$	2.32
839	$6.22\ 10^{-7}$	$6.22\ 10^{+3}$	$6.018\ 10^{+2}$	2.33
932	$6.17\ 10^{-7}$	$6.22\ 10^{+3}$	$6.125\ 10^{+2}$	2.35
1009	$6.17\ 10^{-7}$	$6.22\ 10^{+3}$	$6.189\ 10^{+2}$	2.38
1010	$6.16\ 10^{-7}$	$6.22\ 10^{+3}$	$6.190\ 10^{+2}$	2.37
1013	$6.16\ 10^{-7}$	$6.22\ 10^{+3}$	$6.193\ 10^{+2}$	2.37
1014	$6.17\ 10^{-7}$	$6.22\ 10^{+3}$	$6.194\ 10^{+2}$	2.38
1084	$6.17\ 10^{-7}$	$6.22\ 10^{+3}$	$6.230\ 10^{+2}$	2.39

Table 6 Ion radii of the investigated species as a function of co-ordination number (*CN*)
The ion radius of O^{2-} (r_{O2-}) = 136.4 pm for *CN* = 4, estimated by Shannon & Prewitt[20].

CN	8	7	6	
ion	*r* / pm	*r* / pm	*r* / pm	$-\Delta r \Delta CN^{-1}$ / pm
Zr^{4+}	84	78	72	6
Y^{3+}	101.9	96	90	5.9
Ce^{3+}	114.3	107	101	4.4
Ce^{4+}	97	92	87	5
Er^{3+}	100.4	94.5	89	5.9
U^{4+}	100.0	95	89	5
Pu^{3+}	110*		100	5
Pu^{4+}	96		86	5

* estimated value

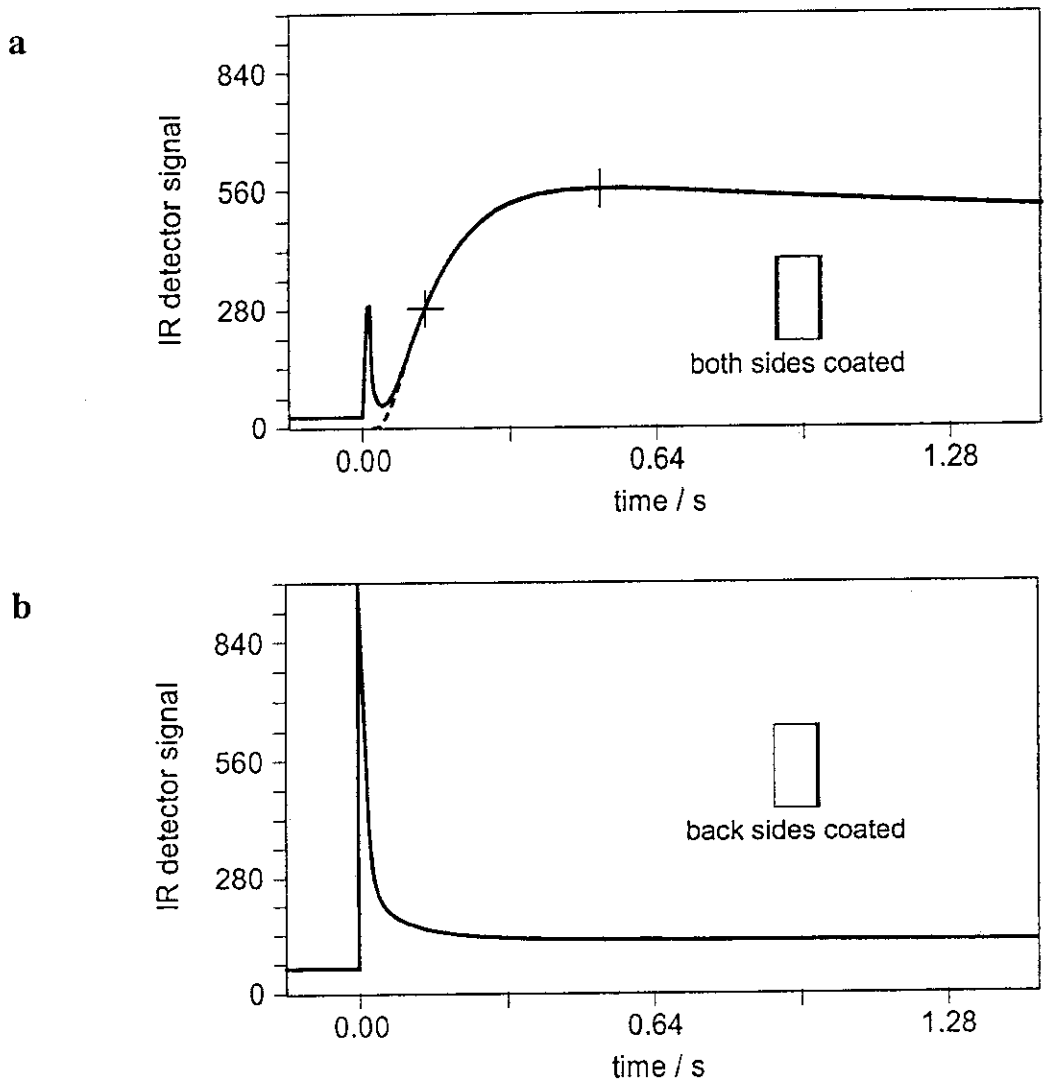

Fig. 1 Effect of the sample preparation on the energy transfer recorded.

a : Classical thermogram obtained with a sample coated on both faces.

b : Thermogram obtained with the sample coated on the detector side only.

Conditions: material, Zr10Y5Er, $d = 9.50\times10^{-3}$ m, $h = 8.3\times10^{-4}$ m.

a

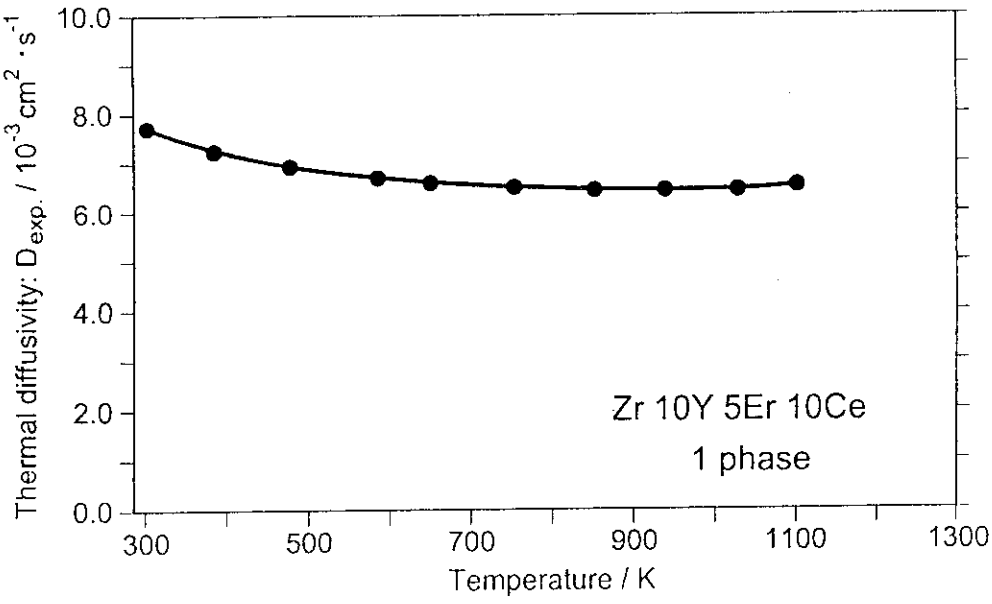

b

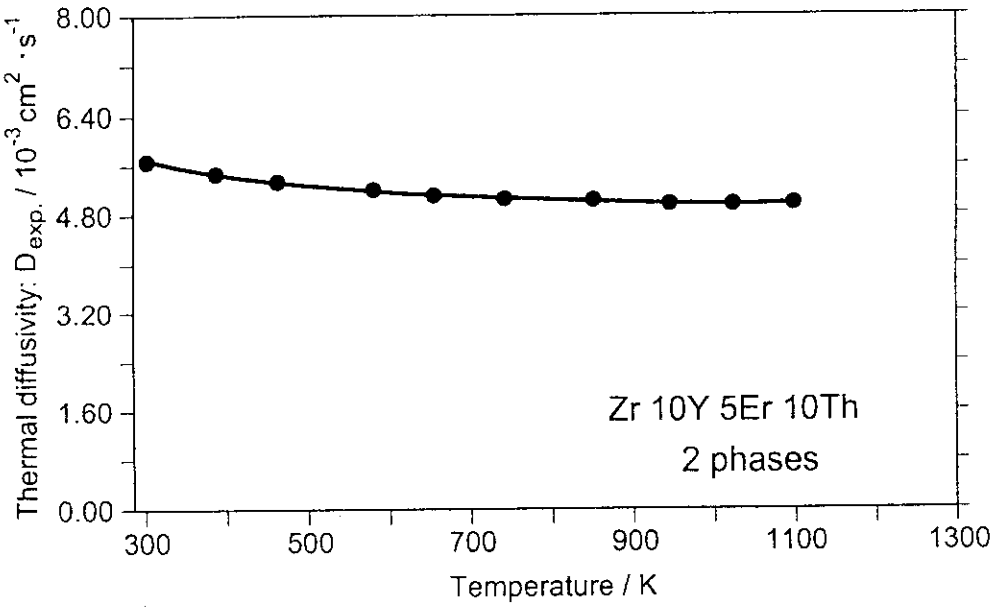

Fig. 2 Experimental thermal diffusivity measured for two quaternary samples.
a : Zr15Y5Er10Ce with single phase.
(diameter 9.60 mm, thickness 0.81 mm, weight 312 mg)
b : Zr15Y5Er10Th, two cubic solid solutions.
(diameter 9.95 mm, thickness 0.82 mm, weight 322 mg)

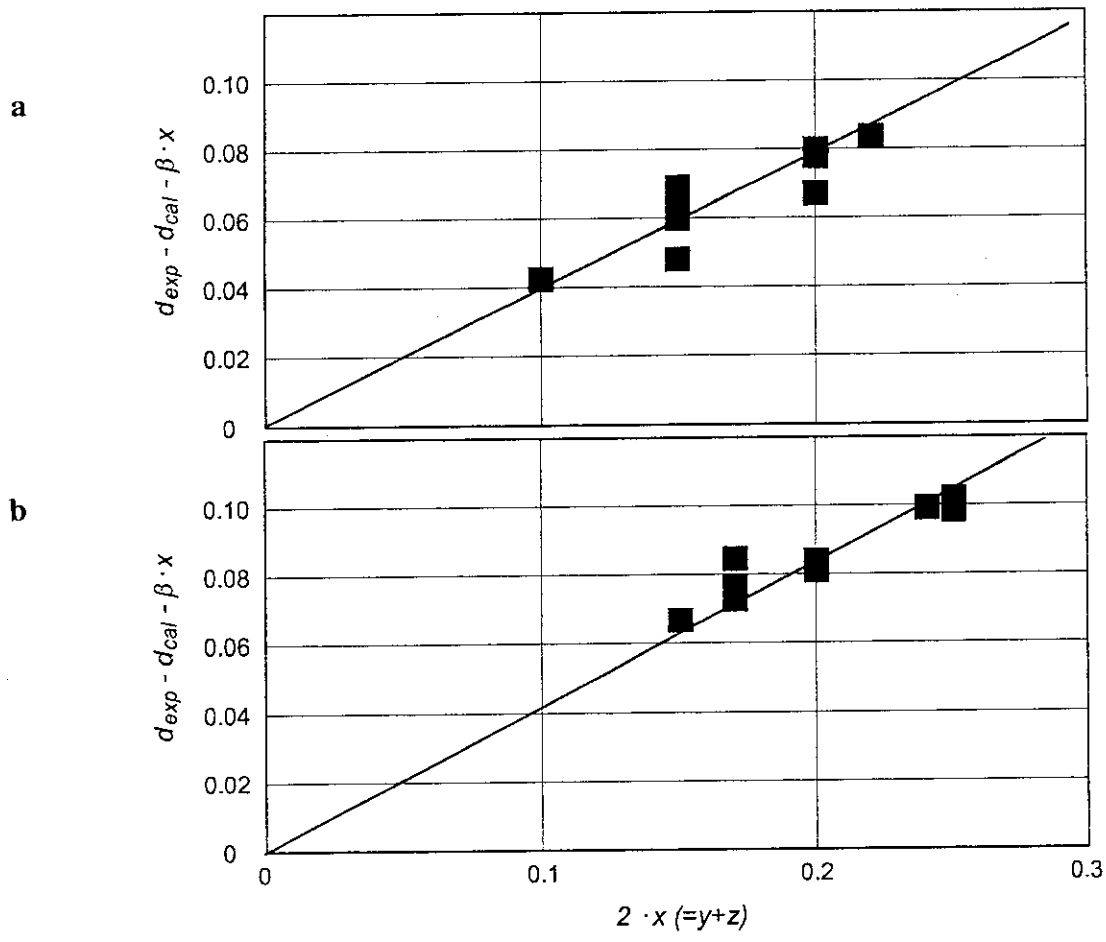

Fig. 3 Effect of yttria and erbia concentrations on the cation - anion distance of zirconia material samples. **a**: without ceria, **b**: with ceria.
Tests based on the experimental d_{exp} and calculated d_{cal} values of the cation-anion distance. Modelling from equation(13).Precision on d: ± 0.5 pm. Note: since $r_Y \approx r_{Er}$ both Y^{3+} and Er^{3+} ions act in a complementary way.

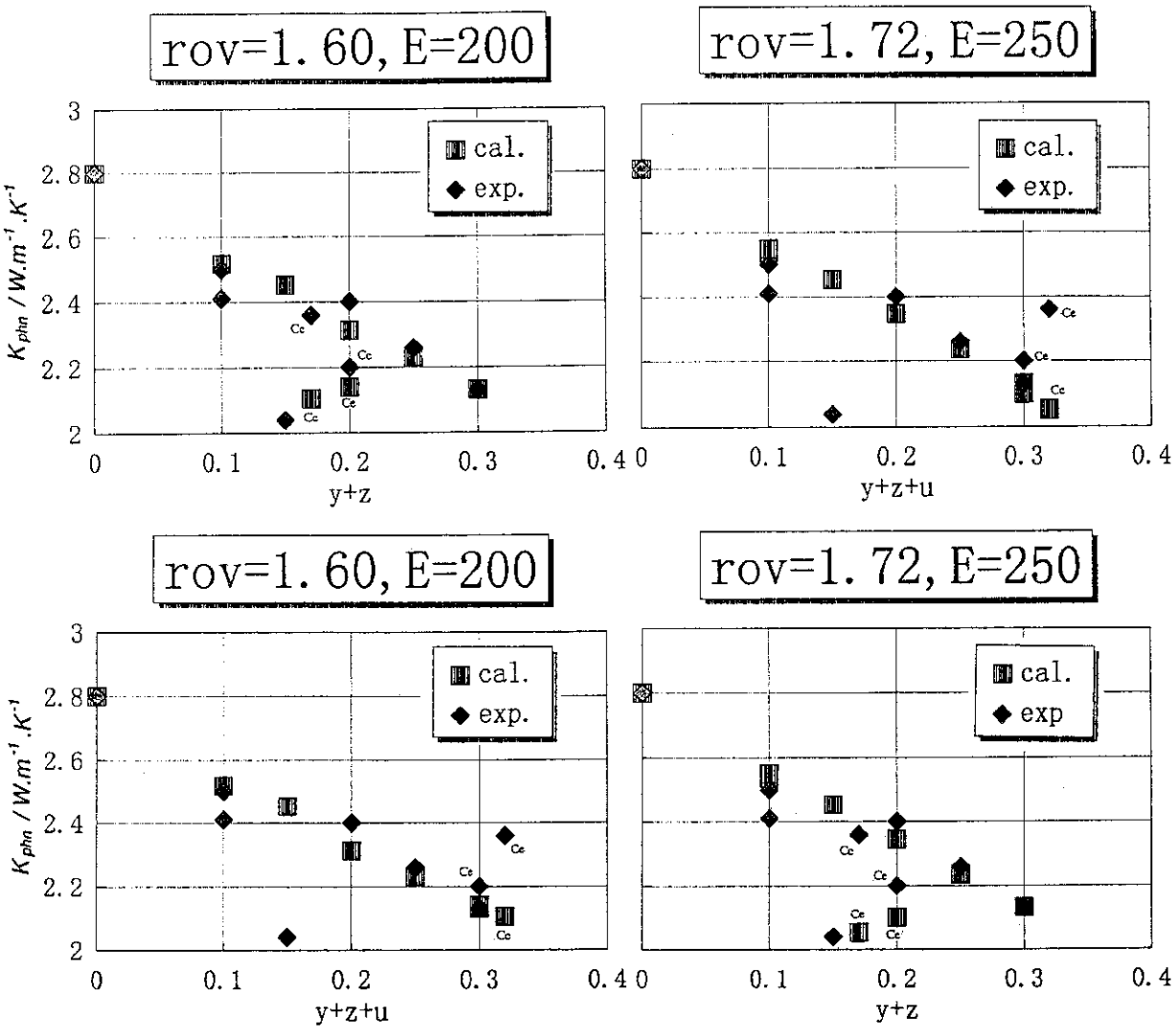

Fig. 4 Effect of yttria or erbia oxide concentration on the thermal conductivity κ_{phn} of the binary, ternary and quaternary zirconia material. Comparison of the experimental and modelled results. Modelling using equations (15) and (16). The best modelling is obtained for r_{OV} = 160 pm and ε = 200.

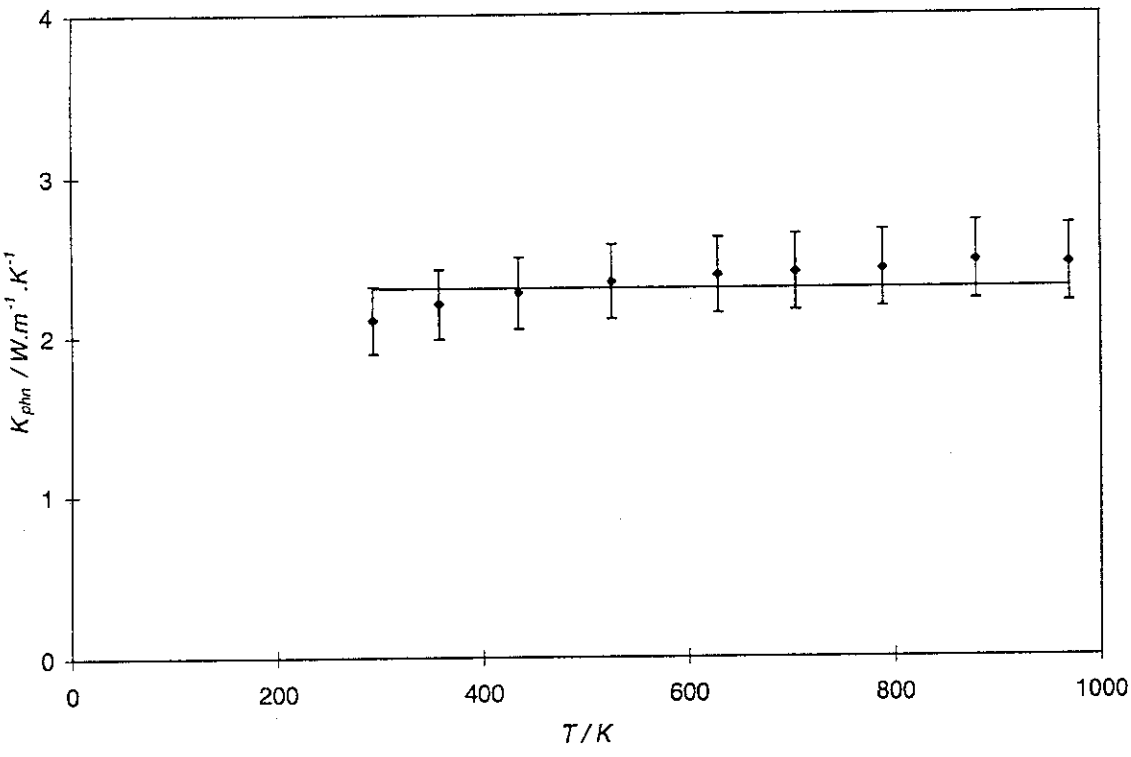

Fig. 5 Effect of temperature on the thermal conductivity of the inert matrix material.
Comparison of the experimental and modelled results. Conductivity parameter obtained from equation (7) and (8), A = 0.435 K·m·W^{-1} and B= 0 m·W^{-1}, sample Zr10Y5Er.

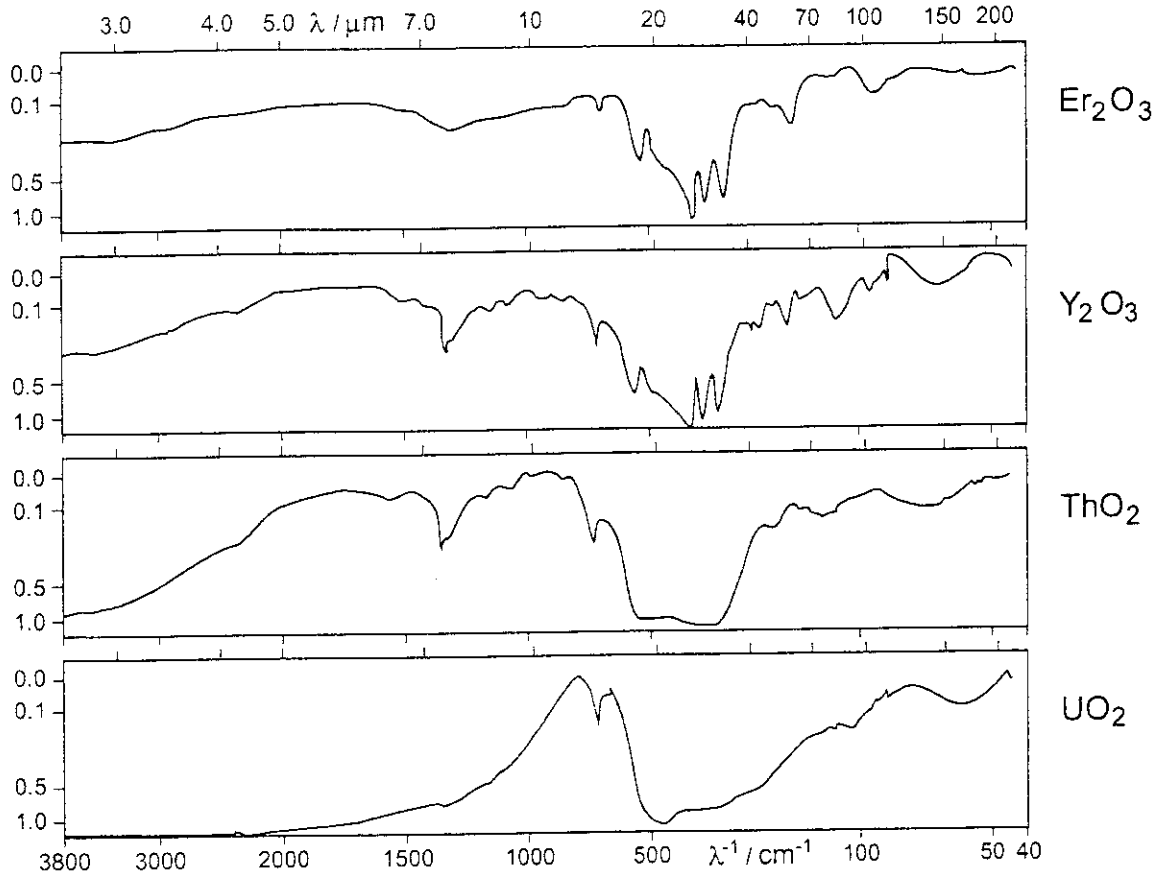

Fig. 6 Infrared spectra of pure materials considered in this study.